WEIGHT REDUCTION IN DYNAMICALLY LOADED SYSTEMS THROUGH THE EFFECT OF DAMPING IN BOLTED JOINTS

SILAS ROEDIGER[1], CARSTEN KOENKE[2] AND HEIKO BEINERSDORF[3]

[1]MFPA Weimar: Material Research and Testing Institute
Coudraystraße 9, 99423, Weimar, Germany
silas.roediger@mfpa.de and www.mfpa.de

[2]Bauhaus-Universität Weimar, Institute for Structure Mechanics
Marienstraße 15, 99423, Weimar, Germany
carsten.koenke@uni-weimar.de and www.uni-weimar.de/de/bau-und-umwelt/institute/ism/

[3] MFPA Weimar: Material Research and Testing Institute
Coudraystraße 9, 99423, Weimar, Germany
heiko.beinersdorf@mfpa.de and www.mfpa.de

Key words: Structure Dynamics, Contact Problems, FEM, Damping in Joints.

Abstract. In order to reduce vibration amplitudes, the MFPA Weimar is investigating joint damping. The effect is based on the relative displacement between two components between which a surface pressure acts. In this case, the surface pressure is applied by a bolted connection. The damping behavior is dependent on normal force and amplitude. Decay tests clearly show that it is not possible to approximate the curves due to the viscous behavior (exponential decay function). The superposition with Coloumb's friction leads to a new damping model, especially in the initial range. The aim is to set up a numerical model in order to be able to take the local damping effects into account in the development of components. For this purpose, zero-thickness elements (ZTE) are introduced into the joint in the FE simulation and provided with a constitutive model that can represent the energy dissipation. The ZTEs are parameterized as a function of material, surface pressure and surface roughness. The amplitude reduction, which is often achieved by a frequency shift of the natural frequencies via tuned mass dampers, is replaced and thus contributes to lightweight construction.

1 INTRODUCTION

Lightweight constructions are becoming increasingly important in today's applications. For dynamically loaded components, the energy required is directly linked to the mass. Components are therefore optimized in terms of their mass. However, lightweight structures often exhibit large vibration amplitudes under dynamic load due to unfavorable excitation states near resonant frequencies. The vibration behavior of a system essentially depends on the mass, stiffness and damping [1] of the system itself. In addition to their lower mass, lightweight structures often also have a lower stiffness. This results in large vibration amplitudes, which can have a negative effect on functionality, operational safety and fatigue strength or lead to undesirable noise emissions from the components [2].

To counteract this effect, the damping is considered for reducing the amplitude of vibration response. There are several causes of damping. The damping mechanisms are classified into internal and external causes of damping. The external ones are air friction or friction in bearings. The internal ones are categorized according to material dependent damping and damping in joints [3]. Among all damping mechanisms, joint damping has been to be the type of damping that maximizes energy dissipation compared to other damping sources [4]. It is often not possible to influence external damping mechanisms due to boundary conditions. Therefore, the damping in joints are pick it out to reduce the amplitude of vibrations.

Damping in joints is often simplified in engineering models, e.g., by simplified viscous damping models with constant parameters [5]. This is possible by small amplitudes, for increasing amplitudes the damping behavior is vibration-dependent and amplitude-dependent, highly nonlinear. An approximation using conventional models is no longer possible. A new damping model must be defined. Therefore, the nature of joint damping is analyzed in experiments and transferred to the model. Analytical models for practical applications fail quickly due to the strong model reduction. Computer-aided calculation is used as an aid to solve complex problems. One numerical solution method is the finite element method (FEM) for calculating complex components. For this purpose, the damping model is implemented in an FEM element formulation.

An example for an application is a trunk door. In the moment an additional mass (tuned mass damper) is introduced [6]. This mass builds up a second vibration system, which counteracts the system response to be reduced. Thus, this frequency shift measure leads to larger system masses and, therewith tends to make a weight-optimized structure heavier again. An additional mass splits a natural frequency into two frequency amplitudes. By splitting, the energy is divided, and the amplitudes are reduced. This effect only applies to one natural frequency. In contrast, damping does not lead to a frequency shift, and the dissipation behavior reduces the amplitude [7].

2 EFFECT OF DAMPING IN BOLTED JOINTS

2.1 Description the Local Energy Dissipation in Steady State

The joint damping is caused at micro level by the contact between surface roughnesses and their relative displacement. The contact is created, for example, by a normal force such as the pretensioning of screws and the relative movement is created by vibrations (cf. Figure 1a). Hysteresis is a measure of energy dissipation. It is a function of the frictional force with the relative displacement (cf. Figure 1b). The area of the hysteresis corresponds to the dissipated energy in one oscillation cycle. With small relative displacements, the roughness peaks in the elastic range are deformed, which is referred to as microslip. The hysteresis has an elliptical shape. If the relative displacements increase or the preload forces decrease, the hysteresis opens up into a parallelogram. This is referred to as macro slip [8]. The roughness peaks shift against each other in the plastic range. In macroslip, the curve rises approximately according to a linear function. The energy dissipation is higher in macroslip, which is why this is targeted. The

condition for switching between microslip and macroslip is provided by the friction condition [9].

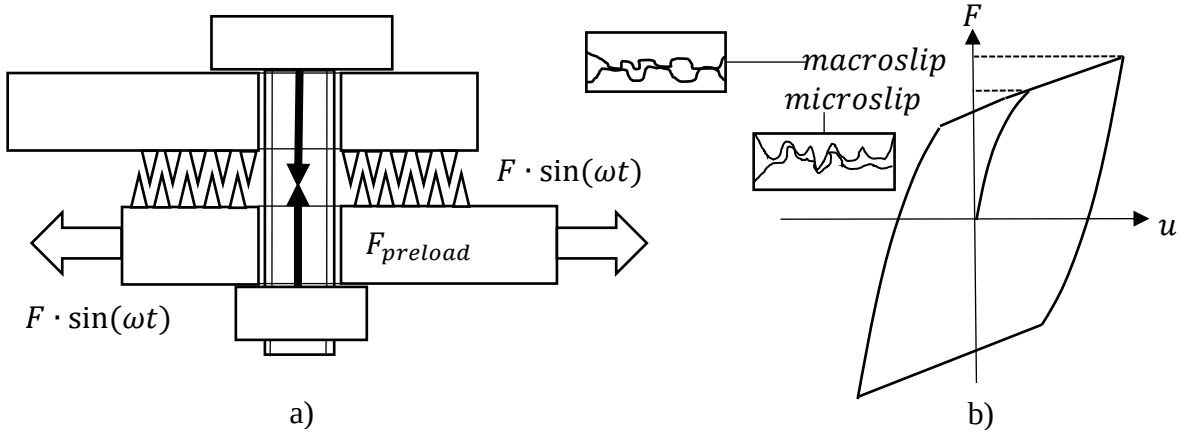

Figure 1: a) Surface interlocking and b) hysteresis

If the force is sufficiently small, there is static friction (microslip), if the force exceeds the switching point, there is sliding friction (macroslip). The energy dissipation in a dynamically loaded system can change over time. On the one hand, due to the external boundary conditions and on the other hand due to tribological changes in the system. The relative displacement causes wear. The roughness peaks are cut. The deformations are associated with the generation of heat and chemical changes to the surface.

Fretting tests are carried out at the Fraunhofer IWM in Karlsruhe to verify the modeling presented. A rounded test specimen and a flat plate are brought into contact. Ideally, this results in point contact. Taking into account the Hertzian pressure, which observed the elasticity of the test specimen, the contact surface forms a circular surface with minimized surface area [10]. Surface pressure values similar to those in a bolted joint are generated. While the plate is firmly fixed, a relative displacement with a sinusoidal curve is applied to the other body using a shaker. A piezoelectric sensor is located at the fixed position of the rounded sample. The displacement generates an electrical voltage that is proportional to the frictional force. For a more detailed description, please refer to [4] and [11]. As the hysteresis is measured in the steady state, the decay behavior is described in the next section.

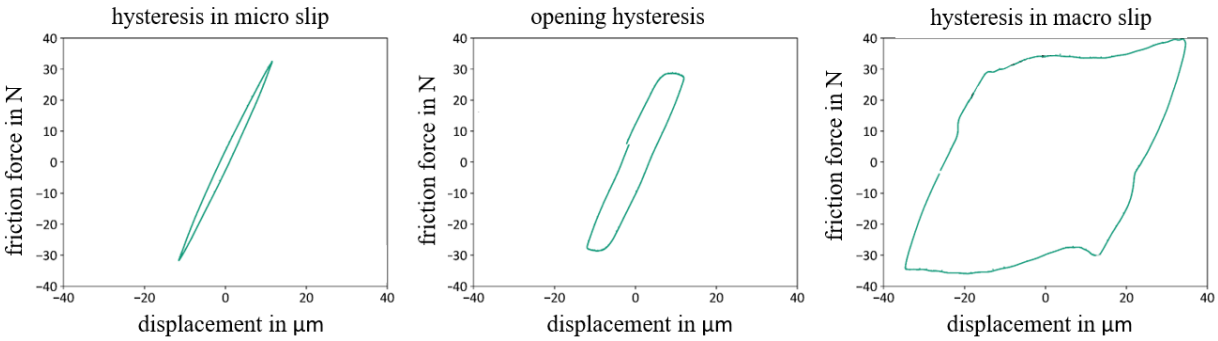

Figure 2: Opening hysteresis, experimental data from Fraunhofer IWM in Karlsruhe, Germany

2.2 Description of Global Damping Behavior

Two hypotheses are examined. The first is that the damping behavior is strongly dependent on the relative displacement and the second is that there is a dependence on the surface pressure. This results in a non-linear behavior. Two L-shaped beams connected by screws, called Brake-Reuss-Beam [12], are considered for evaluation. Different vibration modes, the number of bolts and their preload force are examined. The beam is made of stainless steel and is supported in the vibration minima. The vibration data is recorded using a vibrometer. What makes the beam so interesting is that the joint for the first and second natural frequencies is located at the vibration maximum, whereas for the natural frequencies three and four there are vibration minima. The beam is excited via a impulse at the outer edges according to the respective natural frequency. The impulse force is measured and set in relation to the vibration response to ensure comparability. The transfer function FRF (Frequency Response Function) is thus established. The admittances in graph of Figure 3 is based on the estimation of the transfer function between force excitation and velocity response from the spectral power densities (without averaging over several measurements). The estimator is defined as

$$H1(f) = \frac{Svp(f)}{Spp(f)} \tag{1}$$

where $Svp(f)$ is the complex conjugate of the output spectrum multiplied by the input spectrum and $Spp(f)$ is the complex conjugate of the input spectrum multiplied by itself [13]. First, one bolt with different preload forces (or preload torques) is considered. At natural frequencies 1 and 2, the amplitudes decrease with a lower preload force, thus increasing the damping. The lower preload force allows more relative displacement between the two components, which increases the possibility of macroslip (energy dissipation is significantly higher than in microslip). In contrast, the influence of the preload force on the amplitude reduction for natural frequencies 3 and 4 is less pronounced. As there are vibration minima here, the damping is not significantly increased with the increasing possibility of relative displacements. Remarkable is a small natural frequency shift with the varying preload force.

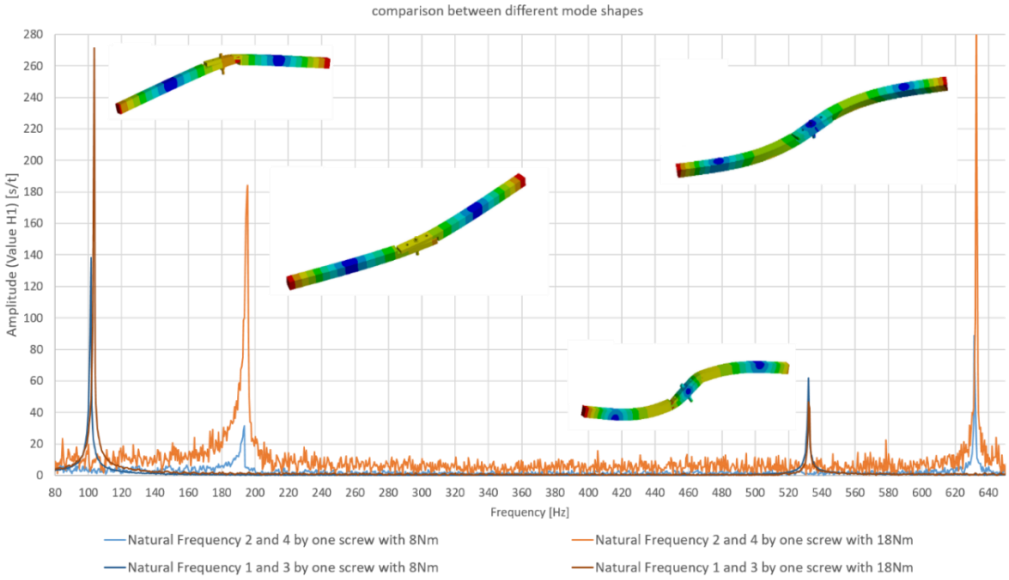

Figure 3: FRF-Function of connected beam by one screw

Decay tests are considered for the evaluation and formation of damping factors, see Figure 4. For this purpose, the structure is excited at the natural frequency using a shaker. By decoupling from the shaker, the drop in amplitudes is observed. If the development of the drop in amplitude is linear, this is referred to as Coloumb behavior. If, on the other hand, the decrease in amplitude corresponds to an exponentially decreasing function, this is pure viscous behavior. Both effects occur simultaneously for the beam. If you look at the beginning of the decay in particular, it becomes clear that the proportion after Coloumb increases as the preload force decreases. A point is formed where the behavior changes to viscous damping. The amplitude is no longer sufficient to generate macroslip. It is similar when increasing the excitation force.

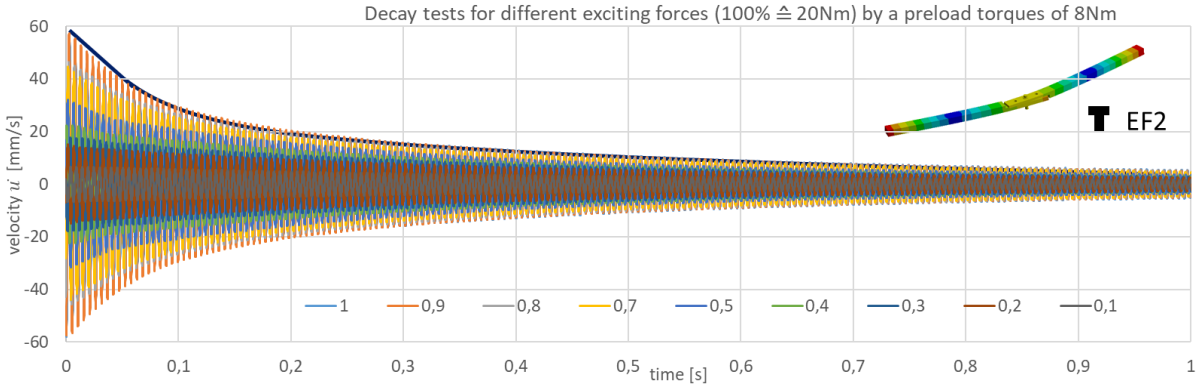

Figure 4: Decay tests for different exciting forces

2.3 Detection of Dissipation Effects in the Joint

As described in the previous section, a point exists at sufficiently high excitation that the viscous behavior is added to the Coloumb component. Two methods are used to detect this point. The first method is the logarithmic decrement over the amplitude. There are formulas for converting the logarithmic decrement into a damping ratio, but this is deliberately omitted because it assumes a specific damping model. According to the effects described, the logarithmic decrement must be constant for a lower amplitude until a threshold value of the amplitude is exceeded. The logarithmic decrement is formed as an example for Figure 5b from

$$\Lambda = ln \frac{\dot{u}_i}{\dot{u}_{i+1}} \tag{2}$$

where $\dot{u}$ is the velocity. Figure 5a indicates that the logarithmic decrement can be assumed to be constant up to an amplitude of approx. 8 mm/s (purely viscous), until the friction component according to Coloumb also increases with an increasing amplitude. This proves the turning point. A smooth transition can be seen for the structure considered here. This is due to the considered oscillation mode of a bending mode tangential to the joining plane. With the additional varying surface pressure (formation of a pressure cone) due to the use of a screw connection, both micro and macroslip can occur simultaneously in the joint plane [2]. The second method is the calculation of the coefficient of determination (COD). All amplitudes converge towards the same value at the end of the decay, although the initial amplitudes start at a higher value with increased excitation. The coefficient of determination R^2 [14] is used for verification. This describes the extent to which the estimation by assuming a function

corresponds to the real values. If this is carried out for all excitation forces, it can be seen that the exponential fit corresponds best at a vibration velocity of approx. until 8 mm/s from right side in each case. This leads to the conclusion that at least viscous behavior occurs at every amplitude. If the value of the amplitude increases, additional behavior according to Coloumb occurs once the coefficient of determination is exceeded. This is equivalent to an opening of the hysteresis in the joint (cf. Figure 2).

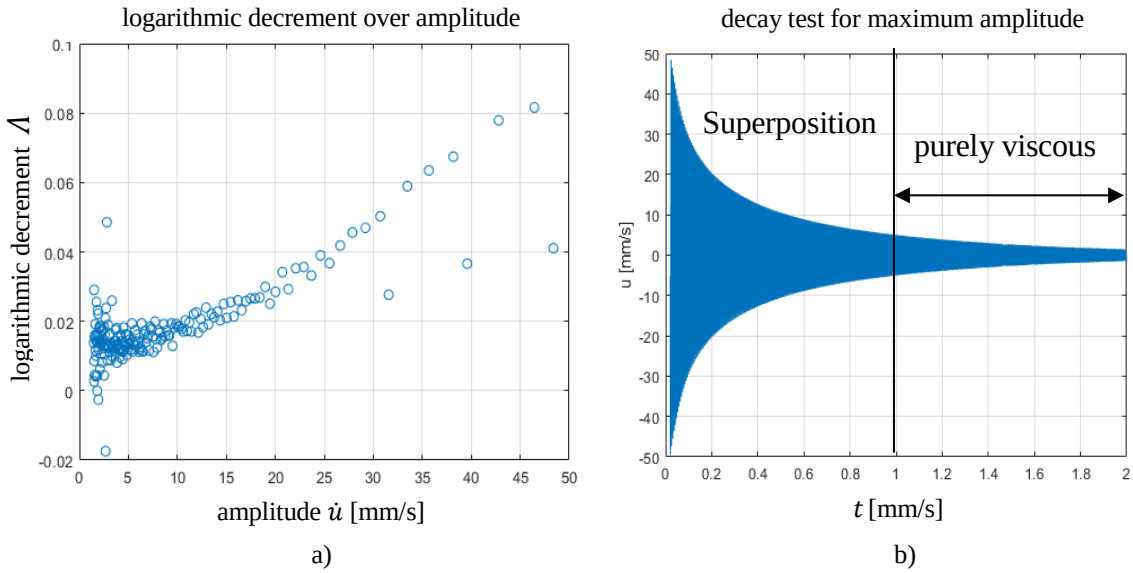

Figure 5: a) Logarithmic decrement over amplitude and b) raw data maximum excitation

The principle of FEM is to be able to describe all effects in 1D and to superimpose them by matrix formation for a 3D structure. For this reason, the derivation of the differential equation of motion for 1D is explained in the following chapter 3.

3 DAMPING MODEL

An attenuation model is derived to illustrate the effects described. First, a 1D vibration is idealized. For the derivation is related to the system to see in Figure 6. The derivation is based on the Lagrange method. It is an energy-based method, which is why it is suitable for the transfer. The general equation is

$$\frac{d}{dt}\left(\frac{\partial L}{\partial \dot{q}_k}\right) - \frac{\partial L}{\partial q_k} = Q^{a*} \tag{3}$$

For a non-conservative system. On the left-hand side, the equation of motion is described without energy dissipation. All energy-dissipative forces are entered on the right-hand side.

$$m_1\ddot{q} + k_1 q = -\frac{\partial D}{\partial \dot{q}_k} + \overrightarrow{F_R}\frac{\partial \vec{r}}{\partial q_k} \tag{4}$$

The Lagrange method is based on generalized coordinates, which are referred to here as q. The dissipation function D is described by the power loss.

$$D = \frac{1}{2}P_V = \frac{1}{2}d_1{v_d}^2 \tag{5}$$

The derivation according to the generalized coordinate results in

$$-\frac{\partial D}{\partial \dot{q}_k} = -d_1\dot{q} \tag{6}$$

The friction component is described by Coloumb's law

$$\overrightarrow{F_R} = -\mu\left|\vec{N}\right|\frac{\vec{v}}{|\vec{v}|} \tag{7}$$

it follows

$$\overrightarrow{F_R}\frac{\partial \vec{r}}{\partial q_k} = -\mu\, m\, g\, sign\dot{q} \tag{8}$$

A decay test is considered, which is why the right-hand side is set to 0

$$m_1\ddot{q} + d_1\dot{q} + k_1 q + \mu\, m\, g\, sign\dot{q} = 0 \tag{9}$$

An α-parameter is introduced, which enables a stepless transition between both viscous damping and friction according to Coloumb. In addition, all dependencies of the parameters are introduced, resulting in

$$m_1\ddot{q}(t) + d_1\left(\alpha, \hat{q}, F_{preload}\right)\dot{q}(t) + k_1 q(t) + \mu(\beta)F_{preload}(t)sign\,\dot{q}(t) = 0 \tag{10}$$

$$\beta = 1 - \alpha \text{ and } \alpha(\hat{q}(t))$$

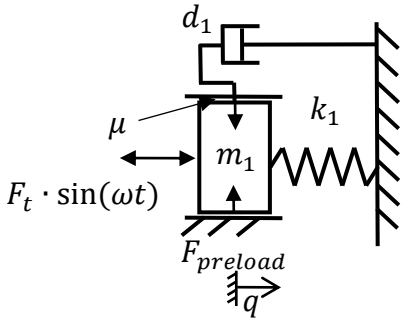

Figure 6: Sketch for derivation of EOM

The basic equation is now known and can be integrated into a model.

4 DAMPING MODEL IN RIGID BODY DYNAMICS

The multi-body model shows the predictive capability of the damping model. Since decay processes are considered in relation to energy dissipation, the simulation is carried out in the time domain. Of particular interest is the motion behavior and not the deformation, which is why a multi-body simulation is used. In contrast to the FEM, the number of bodies/elements considered and their degrees of freedom are reduced, which is why this modeling represents greater computational efficiency in comparison, especially in the time domain. The movement of two bodies is considered. The body above which the oscillation is initiated is referred to as the T-piece, the other as the Pin, shown in Figure 7. With the symmetry condition, only the degree of freedom according to the coordinate system in Figure 7 in the z-direction is released

for the T-piece. A friction joint according to Coloumb is defined between the T-piece and the Pin via the coefficient of friction and normal force application. This releases the relative movement in z. The Pin itself has a joint that allows the normal force to be applied and also leaves the z component free. Three discrete spring and damper elements are used for physical coupling. The spring on the T-piece is fixed. The two remaining discrete elements connect the two bodies together. In the first load step, a displacement with an amplitude of 0.3 mm is applied to the T-piece sinusoidally in the z-direction (this results in a constraint condition) up to 0.04 s and in the second load step the excitation is removed (constraint condition eliminated), resulting in a decay curve. The calculation is carried out explicitly, i.e. the solution is calculated from one time step to the next.

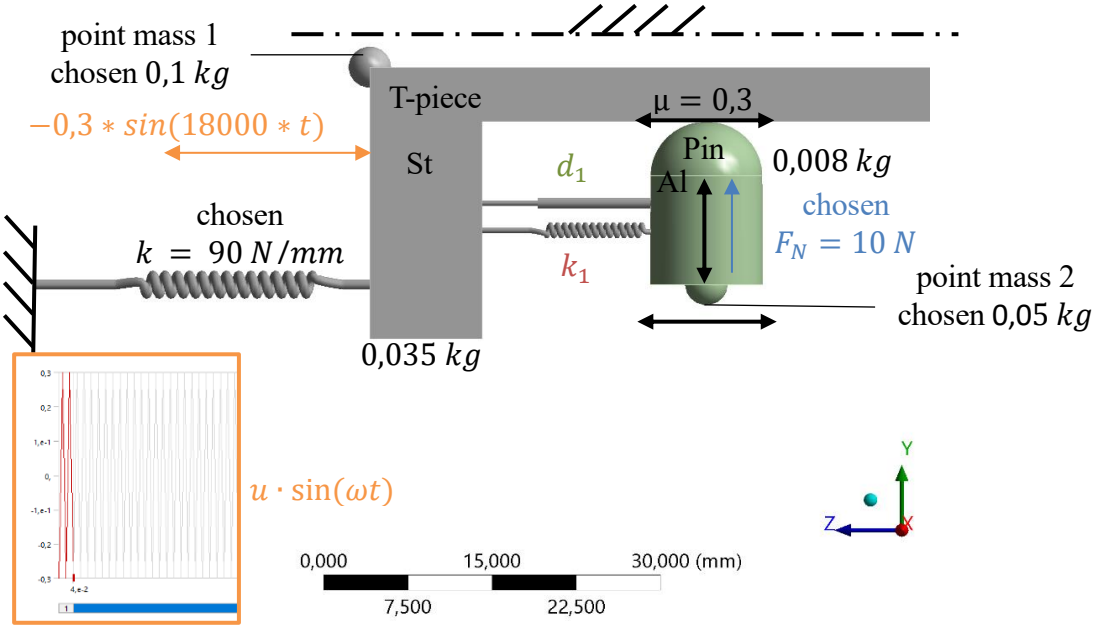

Figure 7: Model of energy dissipation in rigid body dynamics

The color-coded parameters d_1 and k_1 are determined from measured values of hysteresis.

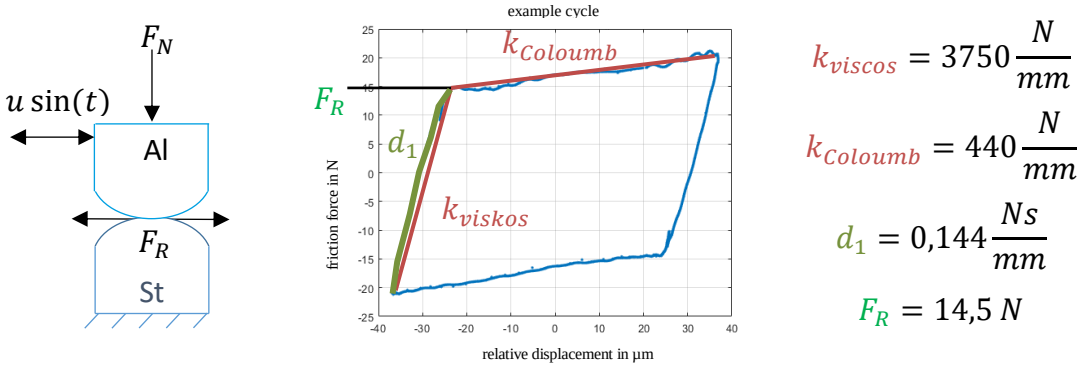

$$k_{viscos} = 3750 \frac{N}{mm}$$

$$k_{Coloumb} = 440 \frac{N}{mm}$$

$$d_1 = 0{,}144 \frac{Ns}{mm}$$

$$F_R = 14{,}5\ N$$

parameter identification of equation (10)

$$m_1\ddot{q}(t) + k_1 q(t) + d_1\left(\alpha(t), \hat{q}, F_{Vorspann}(t), f, MP\right)\dot{q}(t) + F_R(\hat{q}) = 0$$

Figure 8: Parameter identification from experimental fretting test data

The hysteresis recorded is used to determine the limit force, the stiffnesses and the velocity-proportional component. The procedure is demonstrated using an example cycle in Figure 8. The Ansys Rigid Dynamics software is used to set up the differential equations of motion and resolve the matrices. As many differential equations of motion are calculated as the number of generalized coordinates. There are 3 generalized coordinates for this model. After solving, the result data is available in post-processing. The logarithmic decrement is formed in the same way as in Chapter 2.3 and shown in Figure 9. As in the experiments, a turning point can be seen at which the logarithmic decrement changes from a constant value to a linearly increasing value as the amplitude increases.

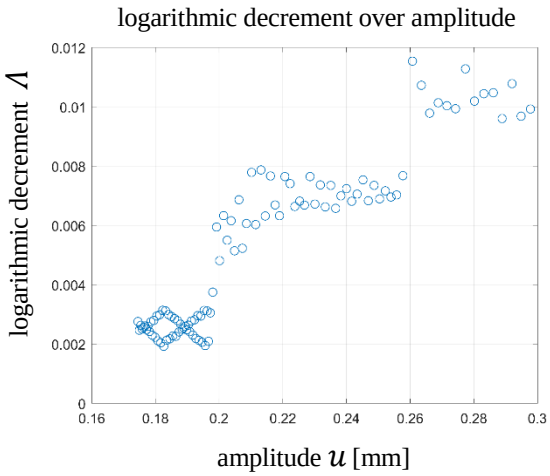

Figure 9: logarithmic decrement from rigid body simulation

The damping model is confirmed in the modeling, the extension to the FEM and thus the consideration of the deformation can take place.

5 OUTLOOK FORMULATION OF FEM-ELEMENT

The equation (10) is now integrated into the global differential equation of motion of an oscillating structure to form

$$M\ddot{u}(t) + \left[D + D(P)^{joint}\right]\dot{u}(t) + \left[K + K(P)^{joint}\right] \bullet u(t) = F \qquad (11)$$

where P are parameters. To take the damping properties into account, the equation must be implemented in an element formulation for the FEM. The modeling of discrete 1D elements requires a search for node pairs, which makes this modeling time-consuming. 2D elements, on the other hand, do not represent a 3D structure. The advantage of 3D elements is that they can be based on simple discretizations such as conformal FE meshes, but this requires identical meshes of the contact partners [15]. Two ways of implementation are considered. One is the formulation using zero-thickness elements (ZTE) and the other is thin-layer elements (TLE) [16], [17]. With TLE, the large thickness-width ratio can lead to numerical problems, as the Jacobian determinant approaches zero for d, i.e. the Jacobian matrix is no longer regular and can no longer be inverted. The focus is therefore on the implementation of a ZTE. According to Figure 10, a trilinear 8-node ZTE is considered, which is constructed from two bilinear 2D quadrilateral elements. Characteristic is d=0.

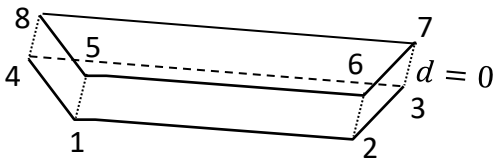

Figure 10: Element formulation of ZTE

The approximation functions are set up for the top and bottom of the element. The element stiffness matrix and damping matrix can be set up by considering the virtual work of the element. The relative displacement results from the subtraction of associated node pairs. The normal behavior is defined in the approximation matrix. For further explanations, please refer to [15], [16], [17].

6 USE CASE BOLTED JOINT

The special feature of a screw connection is that the preload force of the screw forms a pressure cone in the surface of the joined components. This ensures that the possibility of relative displacements is variable depending on the distance to the screw. High normal forces are found in the near of the screw and therefore only small relative displacements occur during vibrations. If the distance to the screw increases, the normal force is reduced. If, for example, the Brake-Reuss beam is considered again at its second natural frequency, this corresponds to a bending vibration parallel to the joining plane. Therefore, a greater relative displacement can be found further away.

An academic example is used to demonstrate the application of damping in bolted joints to reduce amplitudes for plate structures (cf. Figure 11).

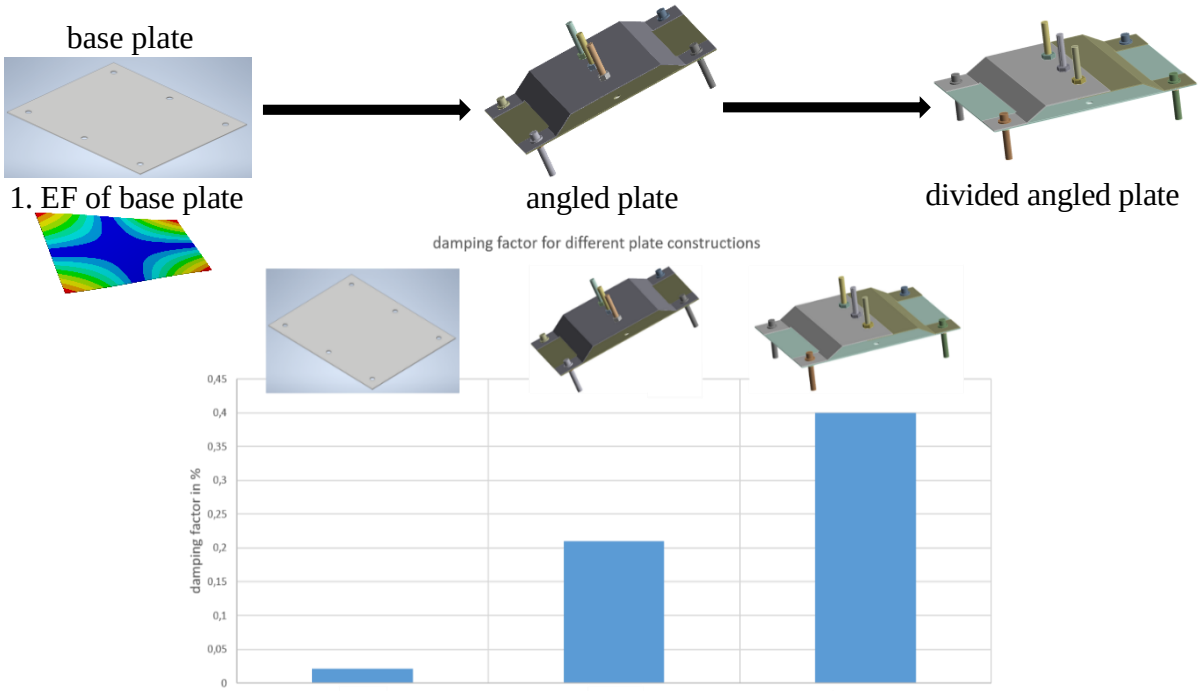

Figure 11: Academic plate construction for experiments and increasing Damping factor

The plate is supported freely and a modal analysis is carried out. The vibration minima are located on half of the edge lengths. In contrast, the vibration maxima are located at the corners of the plates. The idea is to intercept these movements and transfer them to a new plane in which the possibility of relative displacements in particular is permitted. The simpler base plate is shown for the construction. This is bolted together at the four corners using an angled plate. It is important that the base plate is thicker in order to contribute mainly to the swinging properties. In the third stage, the angled plate is divided into two overlapping plates, which are again joined together with screws. This screws are only lightly tightened, while the screws on the base plate are given the full tightening torque.
The proof is provided by experiments. Thin ropes are used to support in the vibration minima. The structure is excited at one corner. Here the excitation takes place acoustically via a loudspeaker, as plate structures tend to have large amplitudes even with a low energy input due to their low stiffness. For better comparability, swing-out curves are considered with the same excitation at the beginning. The curve is linearized by reducing the time considered after the start of the swing-out. This is just 0.4 s. The degree of viscous damping is determined for this period and compared with each other, resulting in the following figure. The base plate achieves an damping factor of 0.02%. The causes of damping here are mainly due to air damping, which accounts for the majority of plane structures without joints. The extension of the structure by the angled plate alone increases the damping to over 0.2%. Relative displacements of the components occur at the joint, which is why the damping is increased here. A further increase in damping is achieved by splitting the angled plate. An additional joint is created, which couples the largest oscillating movements with each other and brings the joining partners into a defined state of friction. Damping factors of over 0.4% are thus achieved for this structure. The experiment shows the application of joint damping and the reduction of amplitudes by utilizing the effect.

7 CONCLUSION

The joint damping achieves the largest damping of all damping types. Due to the conical pressure distribution, micro and macroslip occur simultaneously in a bolted joint. The dependencies of the joint damping depend on the surface pressure and the size of the relative displacement in the joint. A turning point can be found by increasing the amplitude or reducing the preload. The corresponding proof of the local damping effects due to hysteresis could be traced in the global oscillation behavior. At least viscous damping takes place in each cycle with joint damping. After the turning point is exceeded, the friction component according to Coloumb is added to the energy dissipation. This behavior was translated into a mechanical model. The turning point is found at the friction limit at the transition to sliding. ZTE are considered for implementation of damping model. The effect of joint damping in a plate structure was demonstrated in an academic experiment. For this purpose, a plate was divided into two plates and connected by screws trough a base plate. The viscous damping factor was increased by a factor of 2. Joint damping is therefore a way of generating damping effects in lightweight structures while minimizing the increase in mass. The aim is to develop the parameterization and modelling in such a way that validation is no longer necessary and the joint damping is integrated into the virtual development process of a part.

8 ACKNOWLEDGEMENTS

Research funding for this project was provided by Federal Ministry for Economics Affairs and Climate Action (FKZ 03LB2027A) by program TTP LB.

REFERENCES

[1] *VDI 3830 Blatt 1 - Werkstoff- und Bauteildämpfung - Einteilung und Übersicht*. 2004. Accessed: Oct. 27, 2023. [Online]. Available: https://www.vdi.de/richtlinien/details/vdi-3830-blatt-1-werkstoff-und-bauteildaempfung-einteilung-und-uebersicht

[2] H. Wentzel, "Modelling of frictional joints in dynamically loaded structures – a review." Royal Institute of Technology (KTH), 2006.

[3] C. Zacharias, "Numerical Simulation Models for Thermoelastic Damping Effects." Bauhaus-Universität Weimar, Apr. 01, 2022.

[4] S. Rödiger, C. Könke, H. Beinersdorf, and M. Kugler, "Weight reduction in lightweight structures of dynamically loaded systems by new energy dissipative elements in bolted joints," *Eng. Chang. World Proc. 60th ISC*, vol. Ilmenau Scientific Colloquium, p. 2023, Nov. 2023, doi: 10.22032/DBT.58887.

[5] M. Clappier, "Simulation des elektromagnetischen Geräusches einer permanentmagnetisch erregten Synchronmaschine unter Berücksichtigung der Rotordynamik und mechanischer Fügestellen," Graduate School of Excellence advanced Manufacturing Engineering Universität Stuttgart, 2021.

[6] B. Weber and G. Feltrin, "Schwingungstilger – Theoretische Grundlagen und praktische Anwendung." 19. Symposium – Bauwerksdynamik und Erschütterungsmessungen, 2016.

[7] D. Dinkler, *Einführung in die Strukturdynamik*. Wiesbaden: Springer Fachmedien Wiesbaden, 2017. doi: 10.1007/978-3-658-19815-2.

[8] G. Havlicek and G. Kartnig, "Ermittlung des Längsschlupfes eines angetriebenen Kranrads bei bombiertem Schienenkopf," *Vol. 2017*, p. Issue 10, 2017, doi: 10.2195/LJ_PROC_HAVLICEK_DE_201710_01.

[9] F. Bauer, *Tribologie: prägnant und praxisrelevant*. Wiesbaden: Springer Fachmedien Wiesbaden, 2021. doi: 10.1007/978-3-658-32920-4.

[10] Y. Zhou, Y. Xiao, Y. He, and Z. Zhang, "A detailed finite element analysis of composite bolted joint dynamics with multiscale modeling of contacts between rough surfaces," *Compos. Struct.*, vol. 236, p. 111874, Mar. 2020, doi: 10.1016/j.compstruct.2020.111874.

[11] M. Kugler, S. Rödiger, C. Könke, and M. Dienwiebel, "Damping behaviour of different materials in fretting contact - Experiment and simulation using finite element method." 2024.

[12] P. Reuß, "Dynamische Substrukturtechnik unter Berücksichtigung nichtlinearer Interfacekomponenten," *Univ. Stuttg.*, 2020, doi: 10.18419/OPUS-10909.

[13] "What is a Frequency Response Function (FRF)?" Accessed: May 24, 2024. [Online]. Available: https://community.sw.siemens.com/s/article/what-is-a-frequency-response-function-frf

[14] A. Schneider, G. Hommel, and M. Blettner, "Linear Regression Analysis," *Dtsch. Ärztebl. Int.*, Nov. 2010, doi: 10.3238/arztebl.2010.0776.

[15] J. Geisler, "Numerische und experimentelle Untersuchungen zum dynamischen Verhalten von Strukturen mit Fügestellen." Universität Erlangen-Nürnberg, Jan. 01, 2010.

[16] M. H. Mayer and L. Gaul, "Segment-to-segment contact elements for modelling joint interfaces in finite element analysis," *Mech. Syst. Signal Process.*, vol. 21, no. 2, pp. 724–734, Feb. 2007, doi: 10.1016/j.ymssp.2005.10.006.

[17] L. Gaul and M. Mayer, "Modeling of Contact Interfaces in Built-up Structures by Zero-thickness Elements," in *Schwingungen 2017*, VDI Wissensforum GmbH, Ed., VDI Verlag, 2017, pp. 271–286. doi: 10.51202/9783181022955-271.